Trions in semiconducting single-walled carbon nanotubes

Kouta Watanabe and Kenichi Asano*
Department of Physics, Osaka University, Toyonaka, Osaka 560-0043, Japan
(Received 10 September 2011; revised manuscript received 24 November 2011; published 11 January 2012)

We study trions (charged excitons), a complex of an electron-hole pair and an additional electron or hole, in semiconducting single-walled carbon nanotubes (s-SWCNT), by means of the exact diagonalization of the realistic Hamiltonian based on the $\boldsymbol{k}\cdot\boldsymbol{p}$ scheme and on the screened Hartree-Fock approximation. By comparing different classes of models that partially or fully include the band nonparabolicity, the form factors in the density operators, the screening effects on interaction, and the self-energy correction in the energy bands, we succeed in capturing the essential features of s-SWCNT. It turns out that the trion binding energy is significantly suppressed by the form factor as well as by the screening effect. Further, an unconventional feature of s-SWCNT is found: the trion has a larger binding energy than the biexciton, since the biexcitons are more strongly affected by screening than trions. We also consider the effects of the short-range part of the Coulomb interaction, and clarify the fine structures in the trion energy levels. It is shown that the bright (optically allowed) trion with the lowest energy can be interpreted as a bound state of a dark (optically forbidden) exciton and an extra electron or hole.

DOI: 10.1103/PhysRevB.85.035416 PACS number(s): 71.35.Pq, 78.67.Ch

I. INTRODUCTION

Optical properties of semiconductors are often dominated by electron-hole complexes, such as excitons, negative trions (negatively charged excitons), positive trions (positively charged excitons) and biexcitons, which consist of an electron-hole pair, an electron-hole pair with an additional electron, an electron-hole pair with an additional hole, and two electron-hole pairs, respectively. A notable character of quasi-one-dimensional semiconductor systems is strong enhancement of the binding energies of the electron-hole complexes by the spatial confinement effect.[1–14] Among various quasi-one-dimensional systems, the semiconducting single-walled carbon nanotube (s-SWCNT), a rolled monolayer graphite (graphene) with proper chiral vectors,[15,16] has recently attracted particular attention; a huge exciton binding energy is theoretically predicted,[17–20] which is confirmed in experiments.[21,22] The fine structures in the exciton energy levels are also studied both theoretically[23–29] and experimentally.[30–39] Further, a carrier doping of s-SWCNT is realized in two ways: one is the formation of the *p*-*n* junction by the attachment of a pair of split-gate electrodes,[40–44] and the other is the intercalation of the "doner" or "acceptor" molecules.[45–49] It is natural to expect that such doping leads to an emergence of trions with large binding energies. Indeed, quite recently, novel peaks were found in the photoluminescence (PL) measurement in hole-doped s-SWCNT, regardless of the dopant spices.[50] Optical trion generation with the aid of the Auger process is also reported.[51] They are located at 100–200 meV below the bright (optically allowed) exciton peak, and are considered to be the ones from positive trions.

There have been some variational calculations on the trion binding energies in s-SWCNT based on a simplified phenomenological model.[52,53] Still, the theory is lacking an account of the characteristic features of s-SWCNT, namely the band nonparabolicity, the form factors in the density operator, the screening of interaction, and the self-energy correction to the band energies. Note that these features are essential even in a qualitative estimation of the binding energies. In fact, the authors previously reported that the biexciton binding energies are strongly suppressed by the form factors and by the screening of interaction.[54]

In the present paper, the method used to treat excitons[17,18] and biexcitons[54] is applied to trions. All the above features of s-SWCNT, which were missing in the phenomenological models, are taken into account. We also consider the fine structure of the trion energy level, which is induced by the short-range part of the Coulomb interaction. This is required to understand the relative ordering of the bright (optically allowed) and dark (optically forbidden) trion energy levels.

II. FORMULATION

A. $a/L \to 0$ limit

The conduction and valence bands of monolayer graphite (graphene) consist of π orbitals and show a band contact at the K and K′ points, two nonequivalent corners of the hexagonal Brillouin zone. Within the first-order $\boldsymbol{k}\cdot\boldsymbol{p}$ perturbation theory in the vicinity of these two Fermi points, one can express the envelope function of a single electron as a two-component spinor $\boldsymbol{F}(\boldsymbol{r})$ obeying a Weyl (massless Dirac) equation. In s-SWCNT, the wave number of the envelope function in the circumference direction is discretized by the periodic boundary condition, characterized by the chiral index $\nu = \pm 1$.[16] Then, the energies and the envelope functions are given by

$$\epsilon^{\lambda}_{snk} = s\epsilon^{\lambda}_{nk} = s\gamma\sqrt{\left(\kappa^{\lambda}_{n}\right)^2 + k^2}, \tag{1}$$

$$\boldsymbol{F}^{\lambda}_{s,nk}(\boldsymbol{r}) = \frac{1}{\sqrt{AL}}\exp\left[i\left(\kappa^{\lambda}_{n}x + ky\right)\right]\boldsymbol{F}^{\lambda}_{s,nk}, \tag{2}$$

with

$$\kappa^{\lambda}_{n} = \frac{2\pi}{L}\left(n - \frac{\zeta_{\lambda}\nu}{3}\right), \tag{3}$$

$$\boldsymbol{F}^{\lambda}_{s,nk} = \frac{1}{\sqrt{2}}\begin{pmatrix} b^{\lambda}_{nk} \\ s \end{pmatrix}, \qquad b^{\lambda}_{nk} = \frac{\kappa^{\lambda}_{n} - i\zeta_{\lambda}k}{\sqrt{\left(\kappa^{\lambda}_{n}\right)^2 + k^2}}, \tag{4}$$

where we choose the x and y axes as the circumference and the axial direction of the nanotube, $\gamma/\hbar$ denotes the Fermi velocity of the monolayer graphene, and ζ_{λ} is set to $+1$ and -1 for the

two valleys $\lambda = \mathrm{K}$ and K', respectively. The circumference and the axial length of the nanotube are denoted by L and A, respectively, and the conduction and valence bands are distinguished by $s = +1$ and -1, respectively. The integer n is the subband index, k is the axial wave number, and $\sigma = \pm 1$ denotes the electron spin. Note that the wave vector (κ_n, k) is defined for the envelope functions in the vicinity of the valley: the Bloch wave vector of the electron is given by $(K_x^\lambda + \kappa_n, K_y^\lambda + k)$ with the wave vector $\boldsymbol{K}^\lambda$ at the $\lambda = \mathrm{K}$ and K' points. In fact, Eq. (3) is derived from the periodic boundary condition $\exp[i(\kappa_n + K_x^\lambda)L] = \exp(i\kappa_n L + 2\pi i \zeta_\lambda \nu/3) = 1$.

The above effective-mass description of the electron holds in the limit of $a/L \to 0$, where a is the lattice constant. Now, let us proceed to the many-body problem in this limit. Simple dimensional analysis shows that all physical quantities become universal if the length and energy are scaled by L and $2\pi\gamma/L$, respectively.[17] In fact, this limit is specified only by a single dimensionless Coulomb coupling constant,

$$v_c = \left(\frac{e^2}{\epsilon_b L}\right)\left(\frac{2\pi\gamma}{L}\right)^{-1} = \frac{e^2}{2\pi\gamma\epsilon_b} \sim \frac{0.3545}{\epsilon_b}, \tag{5}$$

where e is the elementary charge, and we use $\gamma = 6.46$ eV Å. The background dielectric constant ϵ_b denotes the all contributions *except those from the valence electrons in the vicinity of the Fermi level*, and is affected by the environment where s-SWCNT is placed. Hereafter, we treat $v_c \lesssim 0.25$ as a parameter, assuming that the background dielectric constant is not far from that of graphite, $\epsilon_b \sim 2.4$.[55] In fact, the previous calculation[56] succeeded in evaluating the exciton energies semiquantitatively using $\epsilon_b = 2$. The ratio of the Coulomb energy to the band gap is roughly given by v_c, and is of the order of 0.1, which is a characteristic feature of s-SWCNT. In contrast, in conventional semiconductors, the electron-hole Coulomb interaction is negligibly small compared to the band-gap energy.

Thus, v_c is not negligible, and we have to consider the many-body effects. For this purpose, we introduce here (quasi)electrons and (quasi)holes renormalized in their energies and interactions. The interaction renormalization, namely the screening effect, is considered by the dielectric function based on the random phase approximation (RPA),[17]

$$\epsilon_{m,q} = 1 + u_{m,q}\Pi_{m,q}, \tag{6}$$

where the Fourier component of the Coulomb interaction, $u_{m,q}$, and the polarization function $\Pi_{m,q}$ are given by

$$u_{mq} = \frac{2e^2}{A\epsilon_b} I_{|m|}\left(\frac{L|q|}{2\pi}\right) K_{|m|}\left(\frac{L|q|}{2\pi}\right), \tag{7}$$

$$\Pi_{m,q} = -2\sum_{s,\alpha,s',\alpha',\lambda} \delta_{m,n-n'}\delta_{q,k-k'} \left|\boldsymbol{F}_{s,\alpha}^{\lambda\dagger}\boldsymbol{F}_{s',\alpha'}^{\lambda}\right|^2 \times \frac{\delta_{s,-1} - \delta_{s',-1}}{s\varepsilon_\alpha^\lambda - s'\varepsilon_{\alpha'}^\lambda + i\delta} g_0\left(\varepsilon_\alpha^\lambda\right) g_0\left(\varepsilon_{\alpha'}^\lambda\right), \tag{8}$$

with the abbreviated index $\alpha = (n,k)$ and the modified Bessel functions of the first and second kind, $I_m(q)$ and $K_m(q)$. The cutoff function is given by $g_0(\varepsilon) = \varepsilon_c^{\alpha_c}/(|\varepsilon|^{\alpha_c} + \varepsilon_c^{\alpha_c})$, with $\varepsilon_c = 10 \times (2\pi\gamma/L)$ and $\alpha_c = 20$.[18,26] The screened interaction satisfies $u_{m,q}/\epsilon_{m,q} = u_{|m|,|q|}/\epsilon_{|m|,|q|}$, reflecting the identity $\Pi_{m,q} = \Pi_{|m|,|q|}$.

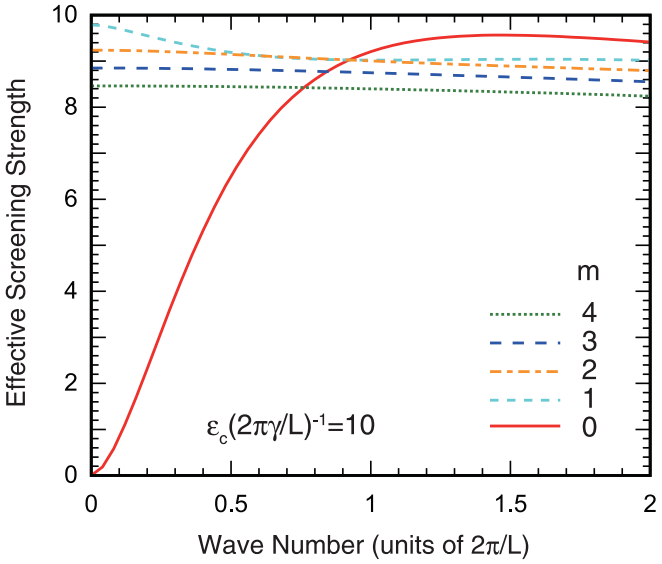

FIG. 1. (Color online) Effective screening strength $u_{m,q}\Pi_{m,q}/v_c$.

Figure 1 shows the evaluated effective screening strength $u_{m,q}\Pi_{m,q}/v_c$. The screening almost vanishes at $m = 0$ and $|q|L \ll 1$; otherwise it has considerable magnitude. This (m,q) dependence of the screening is a characteristic feature of s-SWCNT, which was originally reported in Ref. 17. Indirect evidence of q-dependent screening was also observed experimentally.[57]

The energy of a quasielectron or quasihole is also evaluated as

$$\xi_{n,k}^\lambda = \varepsilon_{n,k}^\lambda + \tfrac{1}{2}\left(\tilde{\Sigma}_{+,n,k}^\lambda - \tilde{\Sigma}_{-,n,k}^\lambda\right), \tag{9}$$

with the (static) screened Hartree-Fock self-energy[17]

$$\tilde{\Sigma}_{s,\alpha}^\lambda = -\sum_{\alpha'} \frac{u_{n-n',k-k'}}{\epsilon_{n-n',k-k'}} \left|\boldsymbol{F}_{s,\alpha}^{\lambda\dagger}\boldsymbol{F}_{-,\alpha'}^{\lambda}\right|^2 g_0\left(\varepsilon_{\alpha'}^\lambda\right), \tag{10}$$

where the electron and hole self-energies are averaged to restore the electron-hole symmetry, which is broken slightly by the cutoff function.[58]

We used above a cutoff function $g_0(\epsilon)$, which contains two parameters ϵ_c and α_c.[17,18] These parameters should be chosen in such a way that only the contributions from the states in the vicinity of the Fermi level, where the $\boldsymbol{k}\cdot\boldsymbol{p}$ approximation holds, are taken into account. The result is insensitive to the choice of α_c, as long as the cutoff function decays smoothly but rapidly enough. The band-gap renormalization, or equivalently the self-energy correction, shows a logarithmic dependence on ϵ_c. However, the binding energies of the electron-hole complexes, which will be discussed below, have no such logarithmic dependence, and do converge unless ϵ_c is too small. We also applied the static approximation to the RPA dielectric function, since it was shown in Ref. 58 that the dynamical effect is irrelevant.

Now, let us consider the complexes of N_e electrons and N_h holes, where (N_e, N_h) is (1,1), (2,1), (1,2), and (2,2) for excitons, negative trions, positive trions, and biexcitons, respectively. Hereafter, we consider only the negative trions,

since they are equivalent to the positively charged ones due to electron-hole symmetry. The Hamiltonian is explicitly written as

$$\mathcal{H} = \mathcal{K} + \mathcal{U}, \tag{11}$$

$$\mathcal{K} = \sum_{\alpha\lambda\sigma} \xi_\alpha^\lambda e_{\alpha\sigma}^{\lambda\dagger} e_{\alpha\sigma}^\lambda + \sum_{\alpha\lambda\sigma} \xi_\alpha^\lambda h_{\alpha\sigma}^{\lambda\dagger} h_{\alpha\sigma}^\lambda, \tag{12}$$

$$\mathcal{U} = \frac{1}{2} \sum_{m,q} \frac{u_{m,q}}{\epsilon_{m,q}} : \left(\rho_{m,q}^{(e)\dagger} - \rho_{m,q}^{(h)\dagger}\right)\left(\rho_{m,q}^{(e)} - \rho_{m,q}^{(h)}\right) :, \tag{13}$$

with the electron and hole density operators

$$\rho_{mq}^{(e)} = \sum_{\alpha,\alpha'\lambda\sigma} \delta_{m,n'-n}\delta_{q,k'-k} f_{\alpha',\alpha}^\lambda e_{\alpha'\sigma}^{\lambda\dagger} e_{\alpha\sigma}^\lambda, \tag{14}$$

$$\rho_{mq}^{(h)} = \sum_{\alpha\alpha'\lambda\sigma} \delta_{-m,n'-n}\delta_{q,k'-k} f_{\alpha',\alpha}^\lambda h_{\alpha'\sigma}^{\lambda\dagger} h_{\alpha\sigma}^\lambda, \tag{15}$$

and the so-called form factor

$$f_{\alpha',\alpha}^\lambda = \boldsymbol{F}_{+,\alpha'}^{\lambda\dagger} \boldsymbol{F}_{+,\alpha}^\lambda, \tag{16}$$

where $e_{nk\sigma}^{\lambda\dagger}$ and $h_{nk\sigma}^{\lambda\dagger}$ create an electron with (n,k,σ,λ) in the conduction subband $(s=+1)$, and a vacancy of an electron (i.e., hole) with $(n,-k,-\sigma,\lambda)$ in the valence subband $(s=-1)$, respectively, and two colons denote the normal ordering of the annihilation and the creation operators inside them.

In the following, we compare the *phenomenological*, *unscreened*, and *screened* models, which are summarized in Table. I. The *phenomenological model* is nothing but the one used previously in the variational and diffusion Monte Carlo calculations,[52,53,59] where the nonparabolicity of the energy bands, the form factors, the screening effect, and the self energy correction are all neglected. This model is reproduced in our scheme by using parabolic dispersion in Eq. (1) and by setting $f_{\alpha',\alpha}^\lambda = 1$, $\Pi_{m,q} = 0$, and $\tilde{\Sigma}_{s,n,k}^\lambda = 0$, in Eqs. (16), (8), and (10), respectively. In the *unscreened model*, the correct nonparabolic energy dispersion of Eq. (1), the form factor of Eq. (16), and the self-energies of Eq. (10) are taken into account, but the screening effect is still neglected. All these features are included finally in the realistic *screened model*.

Once the energy dispersion is corrected from a parabolic to a nonparabolic one, the kinetic energy is reduced and the energies of the electron-hole complex states are lowered. The self-energy correction, by contrast, gives rise to mass reduction and thus raises their energy. Both the form factors and the screening reduce the binding energies as well, since they weaken the electron-hole attractive interaction. Therefore, by comparing these three models, we can understand the competition or cooperation of the effects of the band nonparabolicity, the self-energy correction, the form factor, and the screening of interaction.

TABLE I. Summary of the phenomenological, unscreened, and screened models. The effects considered and neglected in these models are labeled as ◯ and ×, respectively. Enhancement and suppression of binding energies of electron-hole complexes are denoted as ↗ and ↘, respectively.

		Phenomenological	Unscreened	Screened
Nonparabolicity	↗	×	◯	◯
Self-energy	↘	×	◯	◯
Form factor	↘	×	◯	◯
Screening	↘	×	×	◯

B. Corrections to $a/L \to 0$ limit

Since a/L is small but finite in realistic s-SWCNT, the binding energies of the electron-hole complexes, E, should be expanded as a power series of a/L:

$$E\left(\frac{2\pi\gamma}{L}\right)^{-1} = c_0 + c_1\left(\frac{a}{L}\right) + c_2\left(\frac{a}{L}\right)^2 + \cdots, \tag{17}$$

where c_n denotes the coefficient independent of L. The zeroth-order term c_0 is nothing but the contribution from the limit of $a/L \to 0$, and thus depends only on the Coulomb coupling constant v_c. The rest of the terms $(n \geqslant 1)$ express the "fine structures," namely the correction to this limit.

The correction to the interaction term, $\delta\mathcal{U}$, i.e., the short-range part of the Coulomb interaction of the lattice length scale,[26] plays a crucial role in determining the relative ordering of the energy levels of the electron-hole complexes, particularly in thin s-SWCNT. In fact, in nanotubes with diameter $d = L/\pi \sim 1$ nm, it is expected that the energy splittings in the exciton energy levels due to this interaction correction are comparable to the trion or biexciton binding energies. In the second quantized form, the interaction correction term is explicitly written as[60,61]

$$\begin{aligned}\delta\mathcal{U} = {} & \frac{w_1\Omega_0}{2AL} \sum_{m,q} : \left(\bar{\rho}_{mq}^{(e)\dagger} - \bar{\rho}_{mq}^{(h)\dagger}\right)\left(\bar{\rho}_{mq}^{(e)} - \bar{\rho}_{mq}^{(h)}\right) : \\ & + \frac{w_1\Omega_0}{AL} \sum_{m,q} \bar{P}_{mq}^\dagger \bar{P}_{mq} \\ & + \frac{w_2\Omega_0}{AL} \sum_{m,q} : (\bar{\bar{\boldsymbol{\rho}}}_{mq}^{(e)\dagger} - \bar{\bar{\boldsymbol{\rho}}}_{mq}^{(h)\dagger})(\bar{\bar{\boldsymbol{\rho}}}_{mq}^{(e)} - \bar{\bar{\boldsymbol{\rho}}}_{mq}^{(h)}) : \\ & + \frac{w_2\Omega_0}{AL} \sum_{m,q} : \left(\bar{\bar{\boldsymbol{P}}}_{mq}^{(\mathrm{KK}')\dagger} \bar{\bar{\boldsymbol{P}}}_{mq}^{(\mathrm{KK}')} + \bar{\bar{\boldsymbol{P}}}_{mq}^{(\mathrm{K}'\mathrm{K})\dagger} \bar{\bar{\boldsymbol{P}}}_{mq}^{(\mathrm{K}'\mathrm{K})}\right) : \\ & + \sum_{m,q} \frac{u_{mq}}{\epsilon_{mq}} P_{mq}^\dagger P_{mq}, \end{aligned} \tag{18}$$

with

$$P_{mq} = \sum_{\alpha\alpha'\lambda\sigma} \delta_{m,n'-n}\delta_{-q,k'+k}\sigma\, g_{\alpha',\alpha}^\lambda h_{\alpha'-\sigma}^\lambda e_{\alpha\sigma}^\lambda, \tag{19}$$

$$\bar{\rho}_{mq}^{(e)} = \sum_{\alpha\alpha'\lambda\sigma} \delta_{m,n'-n}\delta_{q,k'-k} \bar{f}_{\alpha',\alpha}^\lambda e_{\alpha'\sigma}^{\lambda\dagger} e_{\alpha\sigma}^\lambda, \tag{20}$$

$$\bar{\rho}_{mq}^{(h)} = \sum_{\alpha\alpha'\lambda\sigma} \delta_{-m,n'-n}\delta_{q,k'-k} \bar{f}_{\alpha',\alpha}^\lambda h_{\alpha'\sigma}^{\lambda\dagger} h_{\alpha\sigma}^\lambda, \tag{21}$$

$$\bar{P}_{mq} = \sum_{\alpha\alpha'\lambda\sigma} \delta_{m,n'-n}\delta_{-q,k'+k}\sigma\, \bar{g}_{\alpha',\alpha}^\lambda h_{\alpha'-\sigma}^\lambda e_{\alpha\sigma}^\lambda, \tag{22}$$

$$\bar{\bar{\boldsymbol{\rho}}}_{mq}^{(e)} = \sum_{\alpha\alpha'\sigma} \delta_{m,n'-n}\delta_{q,k'-k} \bar{\bar{\boldsymbol{f}}}_{\alpha',\alpha}^{\mathrm{K}'\mathrm{K}} e_{\alpha'\sigma}^{\mathrm{K}'\dagger} e_{\alpha\sigma}^{\mathrm{K}}, \tag{23}$$

$$\bar{\bar{\boldsymbol{\rho}}}_{mq}^{(h)} = \sum_{\alpha\alpha'\sigma} \delta_{-m,n'-n}\delta_{q,k'-k} \bar{\bar{\boldsymbol{f}}}_{\alpha,\alpha'}^{\mathrm{K}\mathrm{K}'} h_{\alpha'\sigma}^{\mathrm{K}\dagger} h_{\alpha\sigma}^{\mathrm{K}'}, \tag{24}$$

$$\bar{\bar{\boldsymbol{P}}}_{mq}^{(\mathrm{KK}')} = \sum_{\alpha,\alpha'\sigma} \delta_{m,n'-n}\delta_{-q,k'+k}\sigma\, \bar{\bar{\boldsymbol{g}}}_{\alpha',\alpha}^{\mathrm{K}'\mathrm{K}} h_{\alpha'-\sigma}^{\mathrm{K}'} e_{\alpha\sigma}^{\mathrm{K}}, \tag{25}$$

$$\bar{\bar{P}}^{(\mathrm{K'K})}_{mq} = \sum_{\alpha\alpha'\sigma} \delta_{m,n'-n}\delta_{q,k'+k}\sigma \bar{\bar{g}}^{\mathrm{K'K}*}_{\alpha',\alpha} e^{\mathrm{K'}\dagger}_{\alpha'\sigma} h^{\mathrm{K}\dagger}_{\alpha-\sigma}, \quad (26)$$

where w_1 and w_2 parametrize the strength of the intra- and inter-valley interactions, respectively, $\Omega_0 = (\sqrt{3}/2)a^2$ denotes the area of the unit cell, and we introduce the coefficients

$$g^{\lambda}_{\alpha',\alpha} = \boldsymbol{F}^{\lambda\mathrm{T}}_{+,\alpha'} \boldsymbol{F}^{\lambda}_{-,\alpha}, \quad (27)$$

$$\bar{f}^{\lambda}_{\alpha',\alpha} = \boldsymbol{F}^{\lambda\dagger}_{+,\alpha'} \hat{\sigma}_z \boldsymbol{F}^{\lambda}_{+,\alpha}, \quad \bar{g}^{\lambda}_{\alpha',\alpha} = \boldsymbol{F}^{\lambda\mathrm{T}}_{+,\alpha'} \hat{\sigma}_z \boldsymbol{F}^{\lambda}_{-,\alpha}, \quad (28)$$

$$\bar{\bar{f}}^{\lambda'\lambda}_{\alpha',\alpha} = \frac{1}{2}\begin{pmatrix} b^{\lambda'*}_{\alpha'} b^{\lambda}_{\alpha} \\ 1 \end{pmatrix}, \quad \bar{\bar{g}}^{\lambda'\lambda}_{\alpha',\alpha} = \frac{1}{2}\begin{pmatrix} b^{\lambda'}_{\alpha'} b^{\lambda}_{\alpha} \\ -1 \end{pmatrix}, \quad (29)$$

using the z component of the Pauli matrix, $\hat{\sigma}_z$. A simple dimensional analysis shows that the nth order correction of $\delta\mathcal{U}$ to the binding energy in Eq. (17) has the form

$$c_n \left(\frac{a}{L}\right)^n = \psi_n\left(\frac{w_1}{w_2}, v_c\right)\left(\frac{w_2\Omega_0}{2\pi\gamma L}\right)^n \quad (30)$$

for $n \geqslant 1$, where ψ_n is a two-variable function.

Now, let us discuss briefly the fine structure that stems from the correction to the kinetic energy, $\delta\mathcal{K}$. It has two origins:[27] one is the higher-order correction in the $\boldsymbol{k}\cdot\boldsymbol{p}$ expansion, e.g., the trigonal warping of the energy band. The other is the curvature of the nanotube, regarded as lattice distortion, which induces effective magnetic flux. It gives rise to the so-called family pattern in the binding energies of electron-hole complexes, which is already studied and is understood in detail in the case of excitons.[27] As expected from the calculations in the phenomenological models,[52,53,59] these two effects can be taken into account through the renormalization of the exciton binding energy B_{X}, and the ratios of the trion and the biexciton binding energies to the exciton one, $B_{\mathrm{X}^{\pm}}/B_{\mathrm{X}}$ and $B_{\mathrm{XX}}/B_{\mathrm{X}}$, are only weakly affected by them. Therefore, we do not discuss this type of correction any more in the following.

C. Symmetry classification

In our model, x and y components of the total Bloch wave vector of the electrons and the holes,

$$K^{\mathrm{tot}}_x \equiv \sum_{i=1}^{N_e}\left(K^{\lambda_i}_x + \kappa_{n_i}\right) + \sum_{j=1}^{N_h}\left(-K^{\lambda_j}_x - \kappa_{n_j}\right), \quad (31)$$

$$K^{\mathrm{tot}}_y \equiv \sum_{i=1}^{N_e}\left(K^{\lambda_i}_y + k_i\right) + \sum_{j=1}^{N_h}\left(-K^{\lambda_j}_y + k_j\right), \quad (32)$$

are conserved, where $1 \leqslant i \leqslant N_e$ and $1 \leqslant j \leqslant N_h$ are the indices of the electrons and the holes. Since $|k|, |\kappa_n| \ll |\boldsymbol{K}^{\lambda}|$, we can see that

$$N^{\mathrm{K}}_c = N^{\mathrm{K}}_e - N^{\mathrm{K}}_h, \quad (33)$$

$$n_{\mathrm{tot}} = \sum_{i=1}^{N_e} n_i - \sum_{i=1}^{N_h} n_j, \quad (34)$$

$$k_{\mathrm{tot}} = \sum_{i=1}^{N_e} k_i + \sum_{i=1}^{N_h} k_j \quad (35)$$

are conserved, where the electron and the hole number in the K valley are denoted by N^{K}_e and N^{K}_h, respectively. In the following, we discuss the electron-hole complexes characterized by

$$n_{\mathrm{tot}} = k_{\mathrm{tot}} = 0, \quad (36)$$

at which they show the lowest energies. The electron-hole complexes characterized by $K^{\mathrm{tot}}_y = 0$, i.e., by $N^{\mathrm{K}}_c = k_{\mathrm{tot}} = 0$, can be further classified by their parities $P = \pm 1$, which are defined for the spatial inversion in the axial direction. The total spin S of the electrons and the holes is also a conserved quantity.

In the limit of $a/L \to 0$, we can expect higher symmetry due to the absence of intervalley scattering and electron-hole exchange processes. In fact, the electron and hole numbers in the K valley, $N^{(\mathrm{K})}_e$ and $N^{(\mathrm{K})}_h$, and the total electron and total hole spins, S_e and S_h, are independently conserved.

Let us mention here briefly the optical selection rules for trions and biexcitons. Absorption of a single photon linearly polarized along the axial direction creates an electron-hole pair with $N^{\mathrm{K}}_c = 0$, $S = 0$, and $P = +1$.[17] The bright (optically allowed) trion is characterized by $N^{\mathrm{K}}_c = 0,1$ and $S = 1/2$, since the trions are created by the photoexcitation of an electron-hole pair in the single-electron system. The two-photon absorption creates a biexciton with $N^{\mathrm{K}}_c = 0$, $S = 0$, and $P = +1$.

III. RESULTS

A. $a/L \to 0$ limit

First, let us discuss our results in the limit of $a/L \to 0$. The trion energies and the wave functions are determined numerically as the ground state of the Hamiltonian (11) for $(N_e, N_h) = (2,1)$ and for the fixed quantum numbers by means of the Lanczos method. In the phenomenological and unscreened models, we choose the cutoff for the wave number to be $k_c \sim 2 \times 2\pi/a_{\mathrm{B}}$, roughly estimating the exciton radius to be $a_{\mathrm{B}} = \hbar/\sqrt{2(m_b/2)B_{\mathrm{X}}}$ from the exciton binding energy B_{X} and from the lowest-subband mass $m_b = 2\pi\hbar^2/3\gamma L$. Meanwhile, in the screened one, we use $k_c = 2 \times 2\pi/L$ for $a_{\mathrm{B}} < L$, considering that the screening suppresses the short-wavelength components of the interaction. The grid spacing of the wave number is set to $\Delta k = 2\pi/A = k_c/50$. The subband cutoffs, $n_c = 0,1,2$, are also introduced to restrict the electron and hole subbands within $|n| \leqslant n_c$.

Throughout this subsection, we focus only the trions with $S_e = 0$ in the K valley, $(N^{\mathrm{K}}_e, N^{\mathrm{K}}_h) = (2,1)$, because their energies are the lowest among the trions with various spin and valley configurations. Whereas, as shown in the inset of Fig. 2(a), the trion energy levels are almost degenerate regarding the valley configurations. The trion binding energies are defined as

$$B_{\mathrm{X}^{\pm}} \equiv \xi^{\mathrm{K}}_{00} + E_{\mathrm{X}} - E_{\mathrm{X}^{\pm}}, \quad (37)$$

where E_{X} and $E_{\mathrm{X}^{\pm}}$ are the energy levels of the exciton and the trion in the K valley, respectively.

Figure 2(a) shows the trion binding energies in the phenomenological, unscreened, and screened models—$B^{(\mathrm{ph})}_{\mathrm{X}^{\pm}}$, $B^{(\mathrm{un})}_{\mathrm{X}^{\pm}}$, and $B^{(\mathrm{sc})}_{\mathrm{X}^{\pm}}$—as functions of v_c for several choices of the subband cutoff n_c. All are monotonously increasing functions of v_c, and they show the ascending order from screened, to

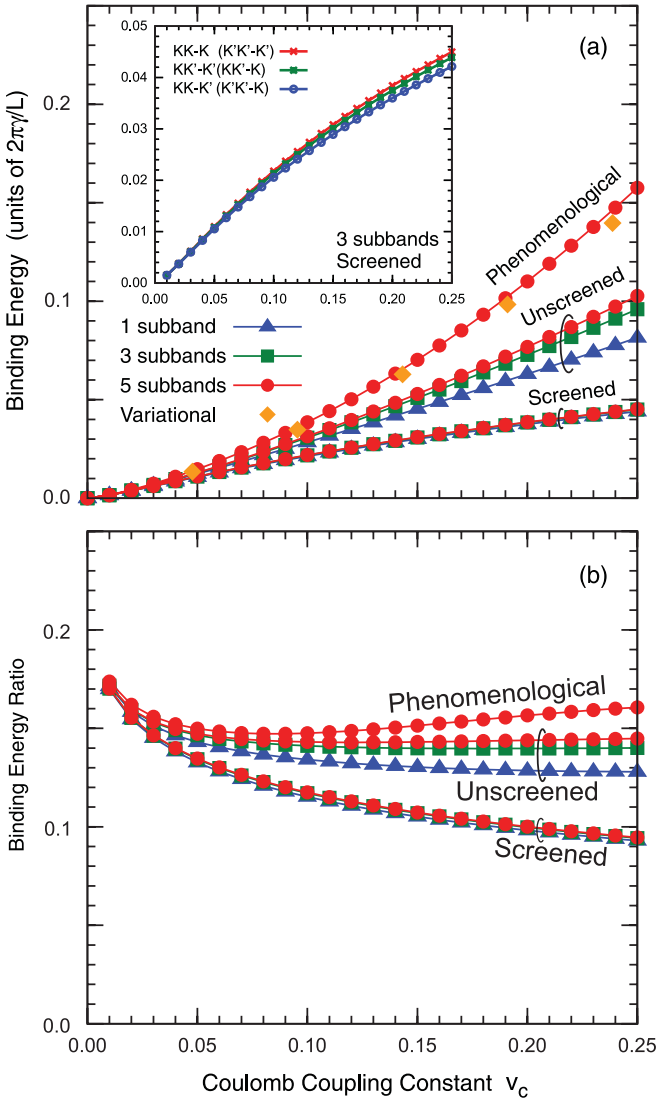

FIG. 2. (Color online) (a) Binding energies $B_{X^\pm}$ of the trion, consisting of two electrons and a hole in the K valley, as functions of the Coulomb coupling constant $v_c = e^2/2\pi\gamma\epsilon_b$, where $\gamma/\hbar$ is the Fermi velocity of graphene and ϵ_b denotes the background dielectric constant. They are calculated in phenomenological, screened, and unscreened models for different subband cutoffs $n_c = 0,1,2$. The result by the variational method in the phenomenological model[52,53] is also shown. Inset: binding energies of trions with different valley configurations, where $\lambda_1\lambda_2$-λ_3 ($\lambda_i = \mathrm{K},\mathrm{K}'$) indicates two electrons and a hole at λ_1, λ_2, and λ_3 valleys, respectively. (b) Binding energy ratio of trion to exciton.

unscreened, to phenomenological models. With increasing degree of intersubband mixing, the trion binding energies become enhanced. At $v_c \lesssim 0.05$, discrepancies among the three models are negligible, which is no longer the case at $v_c \gtrsim 0.05$. It should be noted that our evaluation of $B_{X^\pm}^{(ph)}$ by exact diagonalization is slightly larger and thus more accurate than the previous calculation by the variational method.[52,53]

The trion binding energy is always smaller in the unscreened model than in the phenomenological model, and their difference $B_{X^\pm}^{(ph)} - B_{X^\pm}^{(un)}$ grows as v_c increases. This is mainly because the electron-hole interaction is suppressed by the form factor in the unscreened model. The one in the screened model, $B_{X^\pm}^{(sc)}$, is further reduced from $B_{X^\pm}^{(un)}$, due to the suppression of electron-hole interaction by the screening. $B_{X^\pm}^{(sc)}$ saturates at large v_c, reflecting the saturation of the the screened interaction $u_{m,q}/(1 + u_{m,q}\Pi_{m,q})$ at $u_{m,q} \sim v_c \gg 1$.

Next, one finds that $B_{X^\pm}^{(sc)}$ is almost insensitive to the subband cutoff n_c, whereas $B_{X^\pm}^{(ph)}$ and $B_{X^\pm}^{(un)}$ without the screening effect increase significantly as n_c varies from 0 to 2. This behavior stems from the (m,q) dependence of the dielectric function of Eq. (6) shown in Fig. 1: the screening effect is almost absent in the case of $m = 0$ and $|q|L \ll 1$, while it is relevant for $m \neq 0$ or $|q|L \gtrsim 1$. The suppression of the intersubband interaction ($m \neq 0$) results in the n_c insensitivity of $B_{X^\pm}^{(sc)}$.

In Fig. 2(b), we plot the binding-energy ratio of the trion to the exciton, $B_{X^\pm}/B_X$. At $v_c \gtrsim 0.07$, $B_{X^\pm}^{(ph)}/B_X$ increases monotonously and $B_{X^\pm}^{(un)}/B_X$ is almost unchanged, as functions of v_c. In contrast, $B_{X^\pm}^{(sc)}/B_X$ monotonously decreases. This behavior is again explained by the (m,q) dependence of the dielectric function. Trions have wave functions with more complicate spatial structures, i.e., with more short-wavelength components than excitons. As mentioned above, the screening effect is relevant for the short-wavelength interaction components ($|q|L \gtrsim 1$). Therefore, trions are more sensitive to the screening effect than excitons.

Figures 3 show the electron-electron and electron-hole pair distribution functions, which are defined as

$$g^{(ee)}(x,y) = \frac{1}{AL}\sum_{q,m} \tilde{g}_{m,q}^{(ee)} \exp\left[i\left(\frac{2\pi m}{L}x + qy\right)\right], \quad (38)$$

$$g^{(eh)}(x,y) = \frac{1}{AL}\sum_{q,m} \tilde{g}_{m,q}^{(eh)} \exp\left[i\left(\frac{2\pi m}{L}x + qy\right)\right], \quad (39)$$

with the wave function of the trion, $|\Psi\rangle$, and

$$\tilde{g}_{m,q}^{(ee)} = \frac{1}{N_e(N_e-1)}\langle\Phi| : \rho_{m,q}^{(e)\dagger}\rho_{m,q}^{(e)} : |\Phi\rangle, \quad (40)$$

$$\tilde{g}_{m,q}^{(eh)} = \frac{1}{2N_eN_h}\langle\Phi|\big(: \rho_{m,q}^{(e)\dagger}\rho_{m,q}^{(h)} : + : \rho_{m,q}^{(h)\dagger}\rho_{m,q}^{(e)} : \big)|\Phi\rangle, \quad (41)$$

where x and y denote the coordinates in the circumference and axial directions, respectively. They describe the probability distribution of electrons and holes around the hole at the origin. Note that the hole-hole pair-distribution function $g^{(hh)}$ is equivalent to $g^{(ee)}$ due to electron-hole symmetry.

Figures 3(a) and 3(b) show the y and x dependences of the the electron-hole pair distribution function, respectively. It decreases monotonously as a function of y, indicating that the electrons concentrate around the hole. The degree of concentration is enhanced with increasing v_c. On the other hand, the electrons distribute uniformly along x if we consider only the lowest subband ($n_c = 0$). The inclusion of the excited subbands allows the electrons to concentrate near $x = 0$, whereas its x dependence is too weak to affect the binding energy, as is seen in the small n_c dependence of $B_{X^\pm}^{(sc)}$ in Fig. 2(a).

The y and x dependences of electron-electron pair distribution function are also shown in Figs. 3(c) and 3(d), respectively. The y dependence exhibits a dip at the origin, since the two electrons avoid each other. We can also see that the spatial

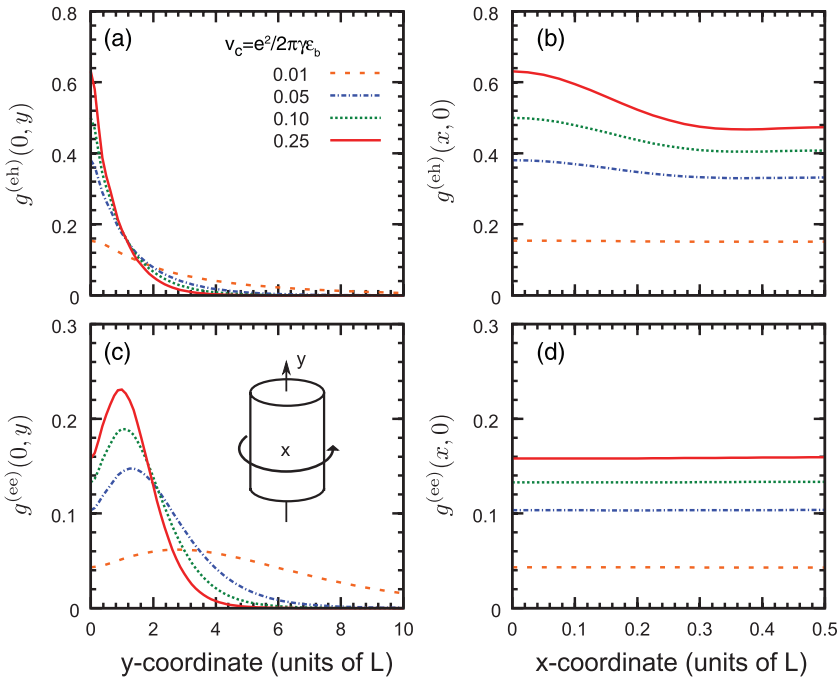

FIG. 3. (Color online) Electron-hole and electron-electron pair distribution functions $g^{(eh)}(x,y)$ and $g^{(ee)}(x,y)$, where x and y axes are chosen in the circumferential and axial directions, respectively. (a) $g^{(eh)}(x=0,y)$. (b) $g^{(eh)}(x,y=0)$. (c) $g^{(ee)}(x=0,y)$. (d) $g^{(ee)}(x,y=0)$.

size of the trion shrinks as v_c is increased. The distribution is almost unchanged and uniform in the x direction, even when we take into account the excited subbands.

Figure 4 shows the v_c dependence of the binding energy difference between the trion and the biexciton, $\Delta \equiv B_{X^\pm} - B_{XX}$, evaluated in the phenomenological, unscreened, and screened models with $n_c = 2$. Here, we use the value of the biexciton binding energy evaluated by the authors,[54] which is defined as

$$B_{XX} \equiv 2E_X - E_{XX}, \tag{42}$$

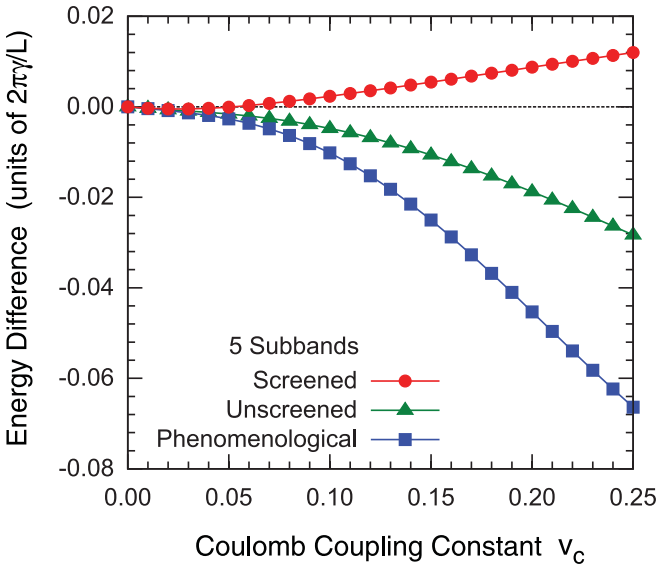

FIG. 4. (Color online) Differences between the trion and biexciton binding energies, $B_{X^\pm} - B_{XX}$, as functions of the Coulomb coupling constant v_c, which are obtained in the phenomenological, screened, and unscreened models with $n_c = 2$.

where E_{XX} denotes the energy level of the biexciton with the quantum numbers $(N_e^K, N_h^K) = (2,2)$ and $(S_e, S_h) = (0,0)$. The ones in the phenomenological and the unscreened models, $\Delta^{(ph)}$ and $\Delta^{(un)}$, both monotonously decrease with v_c, and are always negative. However, the one in the unscreened model, $\Delta^{(sc)}$, increases except at small v_c, and becomes positive at $v_c \gtrsim 0.05$. This implies that the trion peak is located at the lower energy side of the biexciton one in the photoluminescence spectra, which can be explained in terms of the screening effect. As mentioned above, the trion is more sensitive to the screening effects than the exciton. Similarly, the biexciton binding energy is more influenced by screening than the trion one, because of the complicated structure of the biexciton wave function. This is indeed a notable unconventional feature of s-SWCNT. In contrast, it is known theoretically[7–9] and experimentally[11–14] that the binding energies of negative or positive trions are smaller than those of biexcitons in typical quasi-one-dimensional semiconductor systems, e.g., GaAs/AlGaAs quantum wires.

B. Fine structures

Next, let us discuss the fine structures of the trion energy levels caused by the short-range part of the Coulomb interaction, $\delta\mathcal{U}$. We do not use the perturbation theory but diagonalize the full Hamiltonian $\mathcal{H}_{full} = \mathcal{K} + \mathcal{U} + \delta\mathcal{U}$ numerically by the Lanczos method. The subband cutoff is set to $n_c = 0$, since the higher subband mixing effects are negligible in the screened model, as already discussed in the previous subsection.

Here, one should notice that not only the trions but also the excitons are affected by this perturbation, $\delta\mathcal{U}$. Then, the trion binding energies are redefined as

$$B_{X^\pm} \equiv \xi_{00}^K + E_X^{(0,1,+)} - E_{X^\pm}, \tag{43}$$

where $E_{X^\pm}$ denotes the lowest energy level of the trion with a given quantum number, and $E_X^{(0,1,+)}$ is the lowest energy

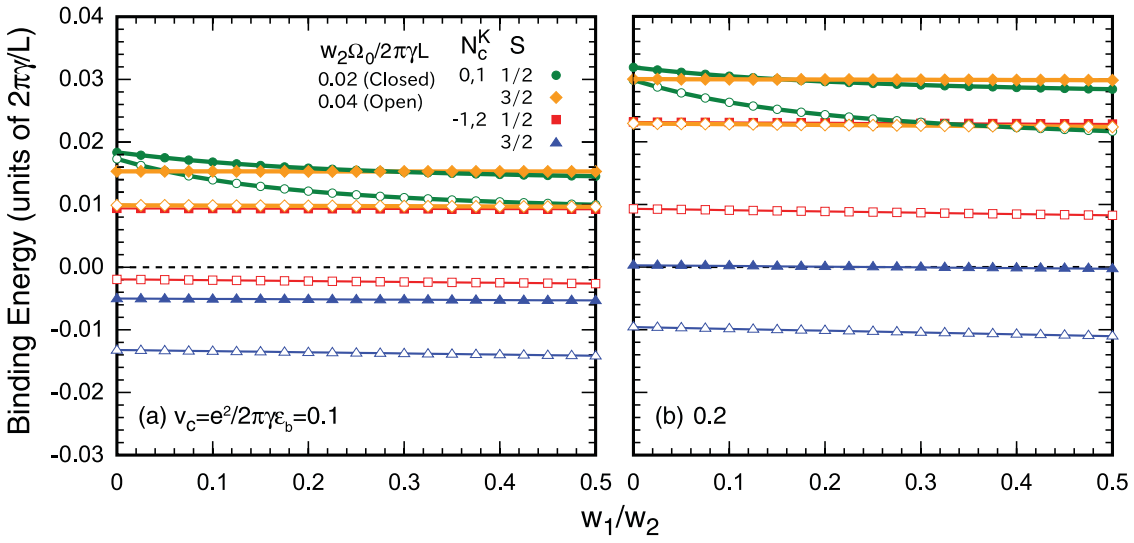

FIG. 5. (Color online) Trion binding energies as function of w_1/w_2, where w_1 and w_2 denote the strength of intra- and inter-valley scattering due to the short-range part of Coulomb interaction, respectively. Trions are classified by their charge number in the K valley, N_c^{K}, and total spin S, and the results at $w_2\Omega_0/2\pi\gamma L = 0.02$ and 0.04 are shown in closed and open symbols, respectively. The Coulomb coupling constant v_c is (a) 0.10 and (b) 0.20.

level of the dark (optically forbidden) exciton with quantum numbers $N_c^{\mathrm{K}} = 0$, $S = 1$, and $P = +1$, which is the true ground state of the electron-hole system of $(N_e, N_h) = (1,1)$. In Fig. 5, the calculated binding energies are shown as functions of w_1/w_2 for the fixed two choices of $w_2\Omega_0/2\pi\gamma L = 0.02$ and 0.04. The trions are classified by their quantum numbers, $(N_c^{\mathrm{K}}, S) = ((0,1),1/2)$, $((0,1),3/2)$, $((-1,2),1/2)$, and $((-1,2),3/2)$, where we use the parentheses in $N_c^{\mathrm{K}} = (n,m)$ to indicate that $N_c^{\mathrm{K}} = n$ and m are equivalent due to inversion symmetry.

We can see that only the bright (optically allowed) trion with $(N_c^{\mathrm{K}}, S) = ((0,1),1/2)$ or the dark one with $(N_c^{\mathrm{K}}, S) = ((0,1),3/2)$ can be the true ground state. In the rest of this subsection, we focus on these two candidates. They always have positive binding energies, and thus can be interpreted as the bound state of the *dark exction* with $N_c^{\mathrm{K}} = 0$, $S = 1$, and $P = +1$, and an electron with spin $1/2$. In fact, the composite of spin 1 and $1/2$ gives a total spin $1/2$ and $3/2$. It is interesting to see that the bright trion is a composite of the dark exciton and an electron. This, however, is natural, since electron-hole recombination is allowed between the additional electron and hole in the dark exciton.

As w_1/w_2 increases, the binding energy of the bright trion is suppressed, while that of the dark one is almost unchanged. Such a difference is caused by the electron-hole exchange process, which raises only the energy level of the bright trion. Actually, this process works between the singlet electron-hole pair, and thus is allowed in the bright trion but is forbidden in the dark one. As a result, the relative ordering of the energy levels between the bright and dark trion is reversed as w_1/w_2 increases. In fact, the bright trion has the lowest energy at small w_1/w_2, while the dark one is the lowest at large w_1/w_2. Similar behavior is also reported for the bright and dark excitons, which are classified by $(N_c^{\mathrm{K}}, S, P) = (0,0,+1)$ and $(0,1,+1)$, respectively.[26]

With increasing $w_2\Omega_0/2\pi\gamma L$, the binding energies of both the bright and dark trions are suppressed. This is presumably attributed to the enhancement of the short-range electron-electron interaction, which works in trions but not in excitons.

IV. SUMMARY AND DISCUSSIONS

In summary, we evaluated theoretically the binding energy and wave function of trions in a semiconducting single-walled carbon nanotube (s-SWCNT) by using a realistic model that properly includes the four different essential features of s-SWCNT: the nonparabolicity in the energy bands, the form factors in the density operator, the screening effects of interaction, and the self-energy correction to the energy bands. By comparing the results of several different classes of models which partially or fully include the above essential features, we succeeded in understanding their role regarding the stability of trions and their optical properties. We showed that the trion binding energy is significantly suppressed by the form factor and by the screening effects, which is the common feature of biexcitons.[54] In particular, we found an unconventional aspect of s-SWCNT: the trion binding energy can exceed the biexciton one, because biexcitons are more sensitive to the screening effect than trions.

The experiment[50] reports that the dependence on the nanotube diameter $d = \pi/L$ on the trion binding energy is given by $B_{\mathrm{X}^{\pm}} \sim C/d + O(d^{-2})$, with $C \sim 60\,\mathrm{meV\,nm}$, if the family pattern effects are not considered. Our numerical evaluation in the limit of $a/L \to 0$ gives $C = 26-52\,\mathrm{meV\,nm}$ for the the Coulomb coupling constant $0.1 \leqslant v_c \leqslant 0.2$. The experimentally measured value is comparable to, but larger than, our evaluation. A possible explanation for this is that the positive trion is loosely bounded around the negatively charged "acceptor" molecule, which leads to the binding energy enhancement in the experiment.

We also investigated the fine structure in the trion energy levels, which is caused by the weak short-range part of the Coulomb interaction. The trions are classified by their charge number in the K valley, by the total spin, and by parity. The bright (optically allowed) trion with the charge number in the K valley of $N_c^{\mathrm{K}} = 0,1$ and the total spin $S = 1/2$, and the dark (optically forbidden) one with $N_c^{\mathrm{K}} = 0,1$ and $S = 3/2$, can always be interpreted as the bound states of the dark exciton and an extra electron or hole. This relative ordering of the bright trion and the dark exciton is confirmed in the experiment.[50] As the relative strength of the intravalley scattering to the intervalley one, w_1/w_2, increases, the binding energy of the bright trion is taken over by that of the dark one. The qualitative understanding of fine structures is still a controversial problem both theoretically and experimentally even for the excitons, and it is hard at present to estimate the explicit values of w_1 and w_2 from the experimental data or first-principles calculations. More quantitative study of the fine structures is left as our future problem.

ACKNOWLEDGMENT

This work was supported in part by KAKENHI (No. 20104010 and No. 21740231), and the Global COE Program (Core Research and Engineering of Advanced Materials–Interdisciplinary Education Center for Materials Science), MEXT, Japan.

*asano@phys.sci.osaka-u.ac.jp

[1] R. Loudon, Am. J. Phys. **27**, 649 (1959).
[2] J. W. Brown and H. N. Spector, Phys. Rev. B **35**, 3009 (1987).
[3] L. Banyai, I. Galbraith, C. Ell, and H. Haug, Phys. Rev. B **36**, 6099 (1987).
[4] T. Ogawa and T. Takagahara, Phys. Rev. B **43**, 14325 (1991).
[5] T. Ogawa and T. Takagahara, Phys. Rev. B **44**, 8138 (1991).
[6] F. L. Madarasz, F. Szmulowicz, F. K. Hopkins, and D. L. Dorsey, Phys. Rev. B **49**, 13528 (1994).
[7] T. Tsuchiya, Int. J. Mod. Phys. B **28**, 3985 (2001).
[8] B. Szafran, T. Chwiej, F. M. Peeters, S. Bednarek, and J. Adamowski, Phys. Rev. B **71**, 235305 (2005).
[9] H. Zhang, M. Shen, and J. Liu, J. Appl. Phys. **103**, 043705 (2008).
[10] M. Kohl, D. Heitmann, P. Grambow, and K. Ploog, Phys. Rev. Lett. **63**, 2124 (1989).
[11] T. Baars, W. Braun, M. Bayer, and A. Forchel, Phys. Rev. B **58**, R1750 (1998).
[12] W. Langbein, H. Gislason, and J. M. Hvam, Phys. Rev. B **60**, 16667 (1999).
[13] H. Akiyama, L. Pfeiffer, A. Pinczuk, K. West, and M. Yoshita, Solid State Commun. **122**, 169 (2002).
[14] Y. Hayamizu, M. Yoshita, Y. Takahashi, H. Akiyama, C. Z. Ning, L. N. Pfeiffer, and K. W. West, Phys. Rev. Lett. **99**, 167403 (2007).
[15] R. Saito, M. Fujita, G. Dresselhaus, and M. Dresselhaus, Appl. Phys. Lett. **60**, 2204 (1992).
[16] H. Ajiki and T. Ando, J. Phys. Soc. Jpn. **62**, 1255 (1993).
[17] T. Ando, J. Phys. Soc. Jpn. **66**, 1066 (1997).
[18] T. Ando, J. Phys. Soc. Jpn. **73**, 3351 (2004).
[19] C. D. Spataru, S. Ismail-Beigi, L. X. Benedict, and S. G. Louie, Phys. Rev. Lett. **92**, 077402 (2004).
[20] V. Perebeinos, J. Tersoff, and P. Avouris, Phys. Rev. Lett. **92**, 257402 (2004).
[21] F. Wang, G. Dukovic, L. Brus, and T. Heinz, Science **308**, 838 (2005).
[22] J. Maultzsch, R. Pomraenke, S. Reich, E. Chang, D. Prezzi, A. Ruini, E. Molinari, M. S. Strano, C. Thomsen, and C. Lienau, Phys. Rev. B **72**, 241402 (2005).
[23] H. Zhao and S. Mazumdar, Phys. Rev. Lett. **93**, 157402 (2004).
[24] C. D. Spataru, S. Ismail-Beigi, R. B. Capaz, and S. G. Louie, Phys. Rev. Lett. **95**, 247402 (2005).
[25] R. B. Capaz, C. D. Spataru, S. Ismail-Beigi, and S. G. Louie, Phys. Rev. B **74**, 121401 (2006).
[26] T. Ando, J. Phys. Soc. Jpn. **75**, 024707 (2006).
[27] T. Ando, J. Phys. Soc. Jpn. **78**, 104703 (2009).
[28] J. Jiang, R. Saito, G. G. Samsonidze, A. Jorio, S. G. Chou, G. Dresselhaus, and M. S. Dresselhaus, Phys. Rev. B **75**, 035407 (2007).
[29] K. Sato, R. Saito, J. Jiang, G. Dresselhaus, and M. S. Dresselhaus, Phys. Rev. B **76**, 195446 (2007).
[30] S. Zaric, G. N. Ostojic, J. Kono, J. Shaver, V. C. Moore, M. S. Strano, R. H. Hauge, R. E. Smalley, and X. Wei, Science **304**, 5674 (2004).
[31] S. Zaric, G. N. Ostojic, J. Kono, J. Shaver, V. C. Moore, M. S. Strano, R. H. Hauge, R. E. Smalley, and X. Wei, Nano Lett. **4**, 2219 (2004).
[32] S. Zaric, G. N. Ostojic, J. Shaver, J. Kono, O. Portugall, P. H. Frings, G. L. J. A. Rikken, M. Furis, S. A. Crooker, X. Wei, V. C. Moore, R. H. Hauge, and R. E. Smalley, Phys. Rev. Lett. **96**, 016406 (2006).
[33] J. Shaver, J. Kono, O. Portugall, V. Krstić, G. L. J. A. Rikken, Y. Miyauchi, S. Maruyama, and V. Perebeinos, Nano Lett. **7**, 1851 (2007).
[34] I. B. Mortimer and R. J. Nicholas, Phys. Rev. Lett. **98**, 027404 (2007).
[35] I. B. Mortimer, L.-J. Li, R. A. Taylor, G. L. J. A. Rikken, O. Portugall, and R. J. Nicholas, Phys. Rev. B **76**, 085404 (2007).
[36] R. Matsunaga, K. Matsuda, and Y. Kanemitsu, Phys. Rev. Lett. **101**, 147404 (2008).
[37] R. Matsunaga, K. Matsuda, and Y. Kanemitsu, Phys. Rev. B **81**, 033401 (2010).
[38] P. M. Vora, X. Tu, E. J. Mele, M. Zheng, and J. M. Kikkawa, Phys. Rev. B **81**, 155123 (2010).
[39] S. Takeyama, H. Suzuki, H. Yokoi, Y. Murakami, and S. Maruyama, Phys. Rev. B **83**, 235405 (2011).
[40] S. Tans, A. Verschueren, and C. Dekker, Nature (London) **393**, 49 (1998).
[41] J. Misewich, R. Martel, P. Avouris, J. Tsang, S. Heinze, and J. Tersoff, Science **300**, 783 (2003).
[42] M. Freitag, J. Chen, J. Tersoff, J. C. Tsang, Q. Fu, J. Liu, and P. Avouris, Phys. Rev. Lett. **93**, 076803 (2004).
[43] J. Chen, V. Perebeinos, M. Freitag, J. Tsang, Q. Fu, J. Liu, and P. Avouris, Science **310**, 1171 (2005).

[44]Y. Nosho, Y. Ohno, S. Kishimoto, and T. Mizutani, Nanotechnology **18**, 415202 (2007).
[45]T. Takenobu, T. Takano, M. Shiraishi, Y. Murakami, M. Ata, H. Kataura, Y. Achiba, and Y. Iwasa, Nature Mater. **2**, 683 (2003).
[46]T. Takenobu, T. Kanbara, N. Akima, T. Takahashi, M. Shiraishi, K. Tsukagoshi, H. Kataura, Y. Aoyagi, and Y. Iwasa, Adv. Mater. **17**, 2430 (2005).
[47]K. Matsuda, Y. Miyauchi, T. Sakashita, and Y. Kanemitsu, Phys. Rev. B **81**, 033409 (2010).
[48]J. Lu, S. Nagase, D. Yu, H. Ye, R. Han, Z. Gao, S. Zhang, and L. Peng, Phys. Rev. Lett. **93**, 116804 (2004).
[49]R. G. A. Veiga and R. H. Miwa, Phys. Rev. B **73**, 245422 (2006).
[50]R. Matsunaga, K. Matsuda, and Y. Kanemitsu, Phys. Rev. Lett. **106**, 037404 (2011).
[51]S. M. Santos, B. Yuma, S. Berciaud, J. Shaver, M. Gallart, P. Gilliot, L. Cognet, and B. Lounis, Phys. Rev. Lett. **107**, 187401 (2011).
[52]T. F. Rønnow, T. G. Pedersen, and H. D. Cornean, Phys. Lett. A **373**, 1478 (2009).
[53]T. F. Rønnow, T. G. Pedersen, and H. D. Cornean, Phys. Rev. B **81**, 205446 (2010).
[54]K. Watanabe and K. Asano, Phys. Rev. B **83**, 115406 (2011).
[55]E. A. Taft and H. R. Philipp, Phys. Rev. **138**, A197 (1965).
[56]J. Jiang, R. Saito, Ge. G. Samsonidze, A. Jorio, S. G. Chou, G. Dresselhaus, and M. S. Dresselhaus, Phys. Rev. B **75**, 035407 (2007).
[57]J. Deslippe, M. Dipoppa, D. Prendergast, M. V. O. Moutinho, R. B. Capaz, and S. G. Louie, Nano Lett. **9**, 1330 (2009).
[58]H. Sakai, H. Suzuura, and T. Ando, J. Phys. Soc. Jpn. **72**, 1698 (2003).
[59]D. Kammerlander, D. Prezzi, G. Goldoni, E. Molinari, and U. Hohenester, Phys. Rev. Lett. **99**, 126806 (2007).
[60]The last term of $\delta\mathcal{U}$ in Eq. (18) stems from the electron-hole exchange process caused by the long-range part of the Coulomb interaction, and thus is regarded as a correction to the zeroth-order term c_0. However, its effect is even smaller than the second term in Eq. (18) for the ordinal values of w_1 and a/L, thus we treat it together with the other higher-order terms.
[61]The interaction corrections to the limit of $a/L \to 0$ also include the Umklapp and Auger processes, which do not conserve the total lattice momentum and the electron and/or hole numbers, respectively. Both of them are neglected in the present study. Since the lattice momentum transfer in the Umklapp processes is twice as large as that of the intervalley scattering processes, its contribution is considered to be much smaller than the intervalley ones. The Auger ones mainly contribute to the lifetimes of the electron-hole complexes.